Electronic Supplementary Material (ESI) for Nanoscale Advances.

Supporting Information for: Optimisation of the Thermoelectric Efficiency of Zirconium Trisulphide Monolayers through Unixial and Biaxial Strain

In this document we present additional tables and figures that are mentioned in the main text.

ϵ_x	1	2	3	4	5	6
-4	1.17	0.90	1.19	2.31	3.36	1.55
-3	1.12	0.97	1.10	1.37	1.56	1.24
-2	1.12	0.97	1.10	1.37	1.56	1.24
-1	1.06	0.98	1.05	1.16	1.23	1.12
0	1.00	1.00	1.00	1.00	1.00	1.00
1	0.94	1.01	0.95	0.88	0.82	0.88
2	0.88	1.02	0.91	0.80	0.68	0.78
3	0.85	1.03	0.86	0.71	-0.14	0.69
4	0.88	1.02	0.91	0.80	0.68	0.78
5	0.88	1.02	0.91	0.80	0.68	0.78
6	0.88	1.02	0.91	0.80	0.68	0.78
7	0.88	1.02	0.91	0.80	0.68	0.78

Table 1: Average relative variation of the six lowest-lying phonon branches between $q = [0.0, 0.0, 0.0]$ and $q = [0.04, 0.0, 0.0]$, with respect to the unstrained case, for uniaxial strains ϵ_x along the x-axis.

ϵ_y	1	2	3	4	5	6
-4	1.02	0.91	1.05	2.74	2.16	1.76
-3	1.07	0.94	1.04	2.04	1.65	1.37
-2	0.84	0.98	1.03	1.48	1.33	1.15
-1	0.94	1.00	1.00	1.09	1.13	1.04
0	1.00	1.00	1.00	1.00	1.00	1.00
1	0.98	1.02	0.98	1.25	0.89	0.98
2	0.97	1.04	0.97	0.61	0.78	0.99
3	0.96	1.06	0.96	1.02	0.72	1.05
4	0.93	1.06	0.94	0.70	0.67	1.19
5	0.91	1.06	0.92	0.84	0.64	1.43
6	0.90	1.06	0.91	1.02	0.63	1.79
7	1.04	1.08	0.90	1.01	0.63	1.63

Table 2: Average relative variation of the six lowest-lying phonon branches between $q = [0.0, 0.0, 0.0]$ and $q = [0.0, 0.04, 0.0]$, with respect to the unstrained case, for uniaxial strains ϵ_y along the y-axis.

ϵ_b	1	2	3	4	5	6
-4	1.22	0.62	1.21	2.08	3.03	1.64
-3	1.19	0.84	1.16	1.64	2.04	1.39
-2	1.02	0.98	0.98	1.01	0.98	0.99
-1	1.07	0.98	1.05	1.15	1.23	1.11
0	1.00	1.00	1.00	1.00	1.00	1.00
1	0.94	1.03	0.95	0.88	0.81	0.88
2	0.88	1.07	0.90	0.80	0.40	0.78
3	0.84	1.09	0.85	0.71	-0.12	0.70
4	0.80	1.10	0.80	0.65	-0.11	0.63
5	0.75	1.11	0.75	0.59	-0.10	0.57
6	0.71	1.11	0.68	0.48	-0.09	0.51
7	0.68	1.12	0.64	0.48	-0.09	0.42

Table 3: Average relative variation of the six lowest-lying phonon branches between $q = [0.0, 0.0, 0.0]$ and $q = [0.04, 0.0, 0.0]$, with respect to the unstrained case, for biaxial strains ϵ_b.

ϵ_b	1	2	3	4	5	6
-4	1.05	0.70	1.02	43.91	1.31	-0.72
-3	1.07	0.86	1.03	6.65	2.25	2.06
-2	1.04	0.98	0.98	0.08	0.98	0.98
-1	0.83	0.98	1.02	1.86	1.20	1.19
0	1.00	1.00	1.00	1.00	1.00	1.00
1	0.98	1.03	0.99	0.72	0.87	0.87
2	0.97	1.06	0.98	0.19	0.76	0.76
3	0.95	1.08	0.96	0.54	-1.24	0.66
4	0.93	1.09	0.95	1.31	-3.76	0.58
5	0.91	1.10	0.93	2.48	-3.51	0.49
6	0.89	1.11	0.92	7.82	-3.25	0.11
7	0.99	1.11	0.91	7.54	-3.95	0.05

Table 4: Average relative variation of the six lowest-lying phonon branches between $q = [0.0, 0.0, 0.0]$ and $q = [0.0, 0.04, 0.0]$, with respect to the unstrained case, for biaxial strains ϵ_b.

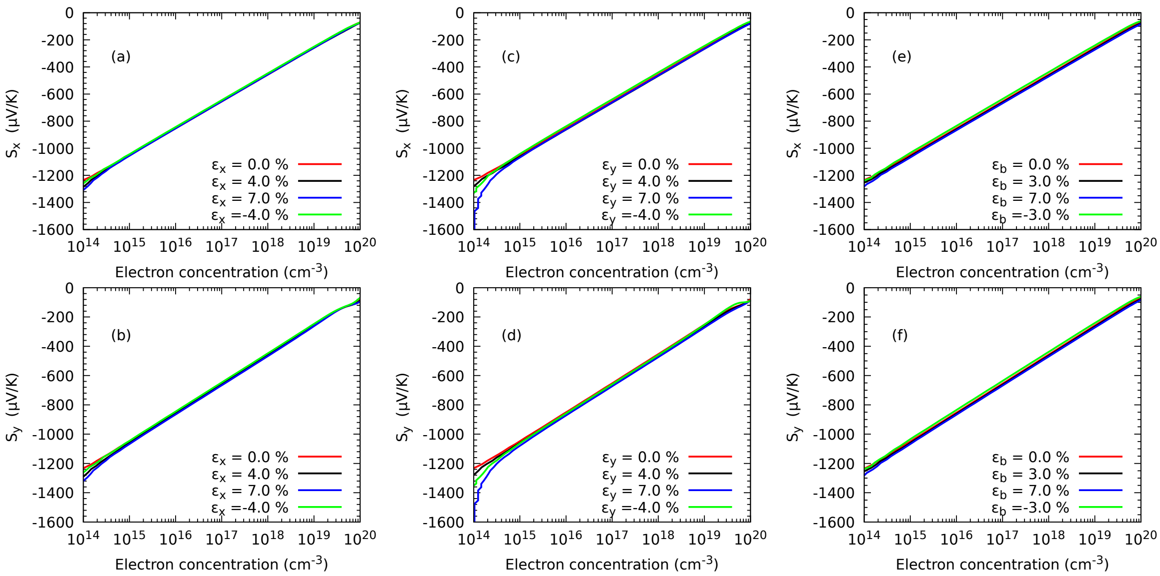

Figure S1: Effect of the electron concentration on the directional Seebeck coefficient S_x (a and c) when strain is applied in the x direction and S_y (b and d) in the y direction and along both axes (e and f) of ZrS_3 monolayers.

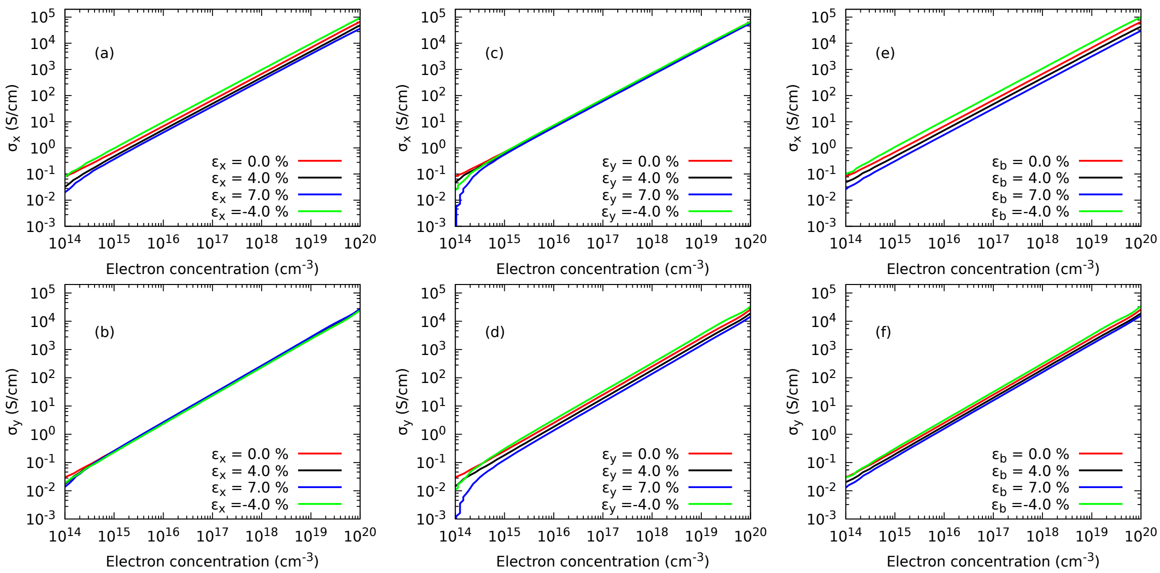

Figure S2: Effect of the electron concentration on the directional electrical conductivity σ_x (a and c) when strain is applied in the x direction and σ_y (b and d) in the y direction and along both axes (e and f) of ZrS_3 monolayers.

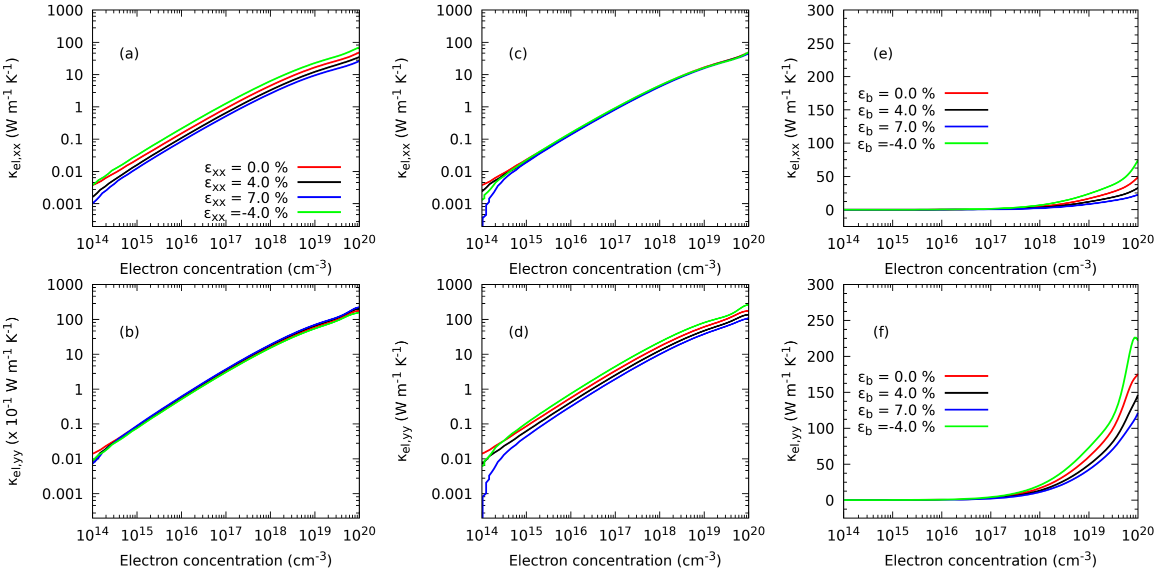

Figure S3: Effect of the electron concentration on the directional electronic contribution to the thermal conductivity $\kappa_{el,xx}$ (a and c) when strain is applied in the x direction and $\kappa_{el,yy}$ (b and d) in the y direction and along both axes (e and f) of ZrS_3 monolayers.

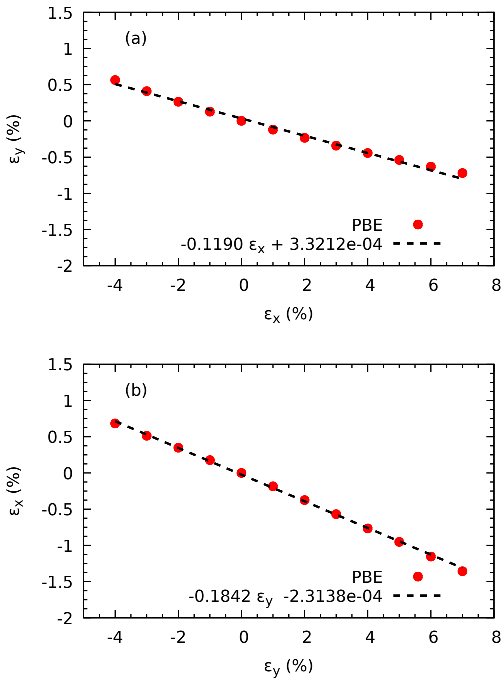

Figure S4: Strains of ZrS_3 monolayer (red dots) in the y (a) and x (b) axis collected at the end of the PBE geometry relaxation upon uniaxial stresses applied along the x and y direction, respectively. Linear fits are made with dashed lines to extract the Poisson's ratio for each direction

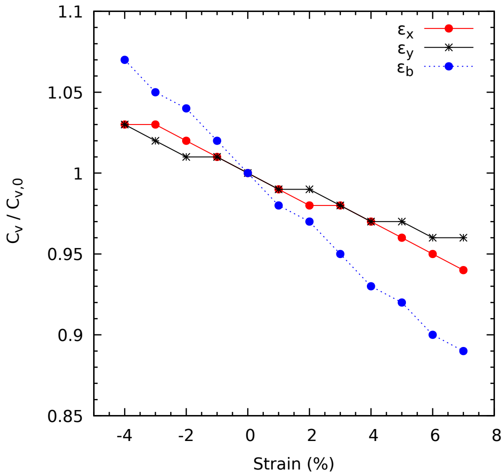

Figure S5: Heat capacity C_v (a and c) when strain is applied in the x direction and $C_{v,y}$ (b and d) in the y direction and along both axes (e and f) of ZrS_3 monolayers.

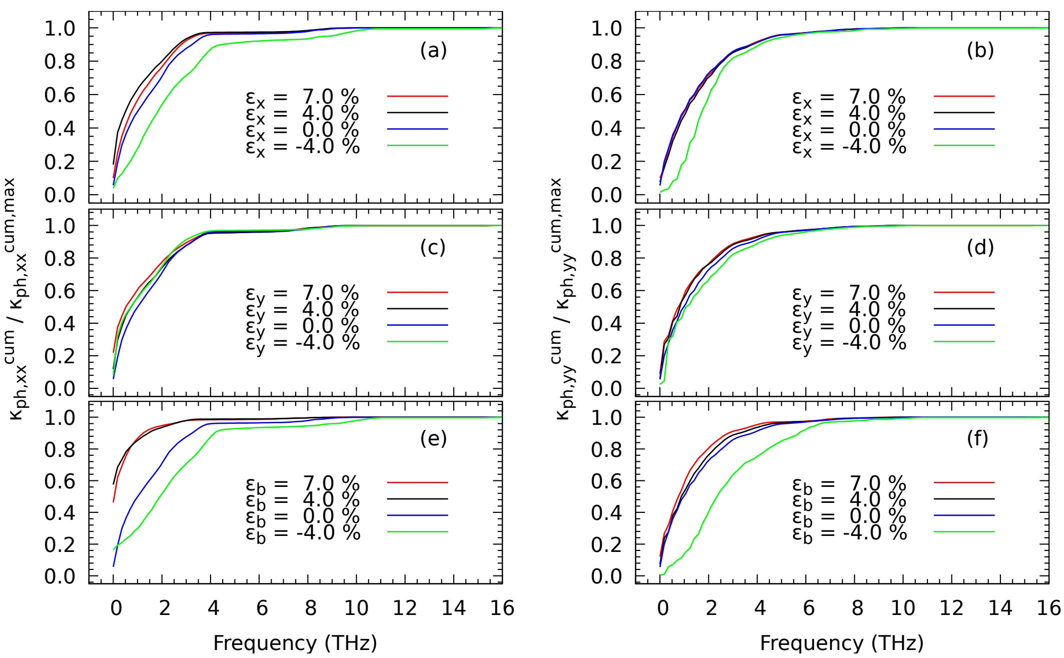

Figure S6: Normalised cumulative function of the components of the tensor of the lattice thermal conductivity $\kappa_{ph,xx}^{cum}$ (panels a, c, and e) and $\kappa_{ph,yy}^{cum}$ (panels b, d, and f) for a number of uniaxial strains ϵ_x and ϵ_y biaxial ϵ_b as a function of the phonon frequency.

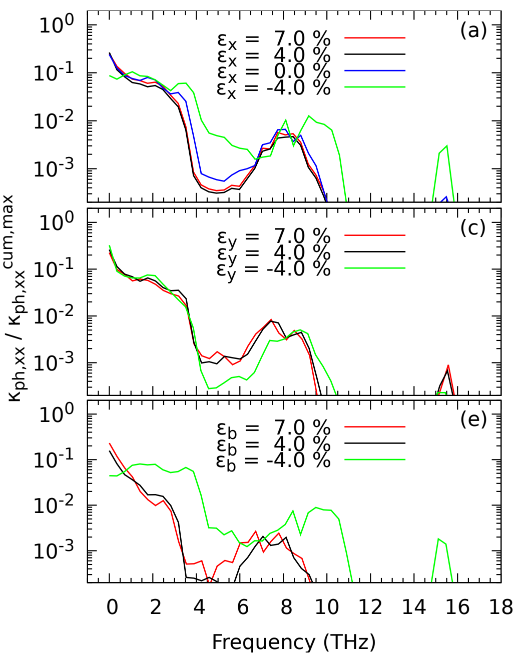

Figure S7: Normalised modal decomposition of the components of the thermal conductivity tensor $\kappa_{ph,xx}^{cum}$ (panels a, c, and e) and $\kappa_{ph,yy}^{cum}$ (panels b, d, and f) for a number of uniaxial strains ϵ_x and ϵ_y biaxial ϵ_b.